High strain-rate material model validation for laser peening simulation

Langer, K. , Olson, S. , Brockman, R. , Braisted, W. , Spradlin, T. and Fitzpatrick, M.E.

High Strain-Rate Material Model Validation for Laser Peening Simulation

Kristina Langer[1], Steven Olson[2], Robert Brockman[2], William Braisted[2], Thomas Spradlin[1], Michael E. Fitzpatrick[3]

[1]*Air Force Research Laboratory, AFRL/RQVS, Wright-Patterson Air Force Base, OH 45433, US*
[2]*University of Dayton Research Laboratory, 300 College Park, Dayton, OH 45469, US*
[3]*Faculty of Engineering and Computing, Coventry University, Priory Street, Coventry CV1 5FB, UK*
E-mail: michael.fitzpatrick@coventry.ac.uk

Published in *The Journal of Engineering*; Received on 1st July 2015; Accepted on 6th July 2015

Abstract: Finite element modeling can be a powerful tool for predicting residual stresses induced by laser peening; however the sign and magnitude of the stress predictions depend strongly on how the material model captures the high strain rate response. Although a Johnson-Cook formulation is often employed, its suitability for modeling phenomena at very high strain rates has not been rigorously evaluated. In this paper, we address the effectiveness of the Johnson-Cook model, with parameters developed from lower strain rate material data ($\sim 10^3$ s^{-1}), to capture the higher strain rate response ($\sim 10^5$–10^6 s^{-1}) encountered during the laser peening process. Published Johnson-Cook parameters extracted from split Hopkinson bar testing were used to predict the shock response of aluminum samples during high-impact flyer plate tests. Additional quasi-static and split Hopkinson bar tests were also conducted to study the model response in the lower strain rate regime. The overall objective of the research was to ascertain whether a material model based on conventional test data (quasi-static compression testing and split Hopkinson bar measurements) can credibly be used in FE simulations to predict laser peen-induced stresses.

1 Introduction

Laser peening (LP) has emerged as a viable and effective surface treatment by which to introduce beneficial compressive stresses into the near surface regions of metallic components. Depending upon the selected peening parameters and application technique, the induced compression can serve to forestall fatigue crack initiation, mitigate fatigue crack growth, or protect against fretting fatigue and stress corrosion cracking [1, 2]. In aircraft applications, laser peening has resulted in airframe fatigue life extension greater than 400% in specific components [3, 4] and has enabled engine blade cost savings surpassing one hundred million US dollars [5].

Currently, development of laser peening solutions for specific applications is highly empirical. Most targeted solution strategies employ destructive techniques for measurement of the LP residual stresses or strains in simple test samples or coupons, which are then used to calculate an LP solution for the actual part of interest (see for example, [6]). While this can be an effective approach for simple geometries that do not differ significantly from the coupons, it does not easily accommodate optimization of LP parameters, nor can it provide detailed distribution of the potentially detrimental compensatory tensile residual stresses. Integrating LP into the part design process – for instance, altering the geometry as a result of peening – is also extremely challenging using empirical methods.

To overcome these design and analysis challenges, physics-based computational models have been developed [7–15]. In this approach, finite element (FE) analysis is used to simulate the LP process and resolve the induced plasticity and residual stresses. The FE models are advantageous in that they can be used to parameterize the LP treatment to achieve an optimized design [10] according to usage constraints. The FE approach also allows for virtual design changes as requirements evolve.

Residual stress predictions from FE modeling depend upon the assumptions used to model the underlying physics, primarily the generation of the laser shock pulse resulting from the laser-matter interaction and the subsequent shock wave motion and material response. While the impact shock can be accurately modeled as a short-duration, high-amplitude mechanical impact, predicting the response of the material to shock wave propagation requires knowledge of the material's strain rate dependence, which is typically not measured during standard material characterization.

In this paper, we address the suitability of using a Johnson-Cook (JC) formulation based on lower strain rate material data ($\sim 10^3$ s^{-1}) to capture the higher strain rate response ($\sim 10^5$–10^6 s^{-1}) encountered during the LP process. Published JC parameters extracted from split-Hopkinson-bar testing were used to predict the shock response of aluminum samples during high-impact flyer plate tests. Additional quasi-static and split-Hopkinson-bar tests were also conducted to study the model response in the lower strain rate regime. The overall objective of the research was to ascertain whether a material model based on conventional test data (quasi-static compression testing and split-Hopkinson-bar measurements) can credibly be used in FE simulations to predict LP-induced stresses.

2 Background

Laser peening is a mechanical surface treatment that uses a high-pressure laser-induced plasma to impart a shock wave into a metallic component. Typical commercial applications employ a short wavelength (~1 μm) Nd-glass or YAG laser with a short pulse duration (~10–100 ns), high power intensity (~1–10 GW/cm^2), and high repetition rate (5–10 Hz) [16]. An ablative medium, such as a black or aluminum tape, is often placed on the component surface prior to peening to boost the plasma formation. A confining medium, such as water, then covers the tape (or the bare metal) to constrain the plasma and increase the impact of the resulting pressure pulse. Good reviews of the LP process can be found in [16] and [17].

The magnitude of the shock pressure on the component surface depends upon the selected laser parameters, but in most cases is on the order of 1-5 GPa with a duration 2–6 times longer than the laser pulse [1]. At these levels of impact, the resulting shock wave can induce strain rates in the components as high as 10^5–10^6 s^{-1}, which can significantly affect the yielding response [18] and hence the formation of residual stresses.

In order to accurately capture these effects in a finite element (FE) simulation, the material model must include strain-rate-dependent yielding, and ideally, should extend from the static or quasi-static case ($\sim 10^{-6}$ s^{-1}) through several orders of magnitude to LP-relevant rates ($\sim 10^5$–10^6 s^{-1}). If the strain rate dependence is excluded from the LP simulations, the predicted residual stress fields are generally more compressive in the near-surface regions, as illustrated in the simple example shown in Figure 1. The

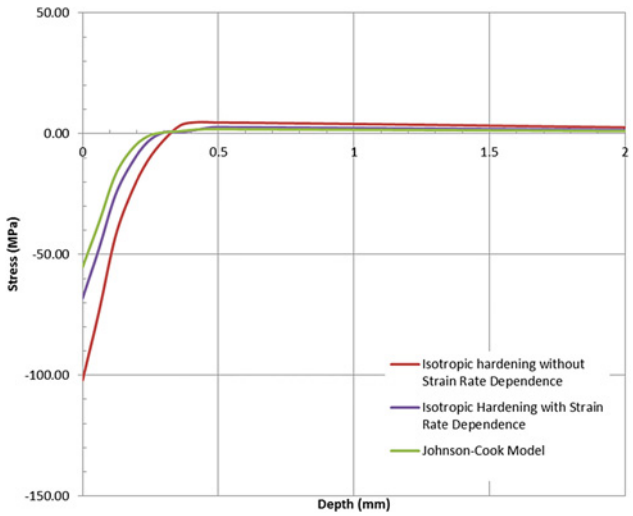

Fig. 1 *Effects of strain rate on predicted residual stress profiles from LP simulation*

predicted residual stress through the thickness of an aluminum plate peened using a single square spot is shown with and without assumed strain rate dependence. As can be seen, when the strain rate is neglected from the material model, the predicted residual stresses near the surface are significantly more compressive than with the strain rate effects taken into account, on the order of about 30–40% greater. This occurs because at these shock pressures, the yield stress increases with strain rate, thereby limiting the plastic deformation and constraining the residual stress.

Although various high strain rate formulations have been proposed, such as those of Bodner [19], Miller [20], Bammann *et al.* [21], and Zerilli and Armstrong [22], the most commonly used for LP aerospace applications is the Johnson-Cook model [23], largely owing to its availability in commercial FE packages. The Johnson-Cook (JC) model was developed in the 1980s as a means to capture the material response during impact and ballistic events. As shown in Equation (1), flow stress $\bar{\sigma}$, is defined as a function of strain hardening and strain rate. (An optional temperature-dependent term is omitted here as earlier studies have demonstrated that thermal effects resulting from the LP process are negligible [24]).

$$\bar{\sigma} = \left[A + B\left(\bar{\varepsilon}^{p}\right)^{n}\right]\left[1 + C\ln\left(\dot{\bar{\varepsilon}}^{p}/\dot{\varepsilon}_{0}\right)\right] \tag{1}$$

Here, $\bar{\varepsilon}^{p}$ is the effective plastic strain; $\dot{\bar{\varepsilon}}^{p}$ is the effective plastic strain rate; $\dot{\varepsilon}_{0}$ is a reference plastic strain rate (typically taken to be 1.0 s^{-1}); n is the work hardening exponent; A is the quasi-static yield strength at room temperature, and B and C are empirically-derived material constants capturing the hardening and strain rate sensitivities, respectively.

Johnson-Cook plots for two common aerospace alloys, Al 2024-T351 and Ti-6Al-4V, are shown in Figure 2. For the aluminum, the strain-rate dependence is fairly moderate. The flow stress increases by about 26% for a strain rate of 10^{6} s^{-1} as compared to a strain rate of 10^{-6} s^{-1}. Although not a large difference, on the order of 100 MPa (15 ksi, approximately), the predicted LP residual stresses can vary significantly if these effects are neglected. The titanium alloy shows a much stronger dependence on strain rate, with an increase of 50% between the quasi-static flow stress and those likely to be experienced during an LP shock event.

The empirical parameters A, B, C, and n in Equation 1 are typically determined using curve fitting techniques with data derived from quasi-static and split Hopkinson bar (SHB) testing [23]. With both test techniques (discussed in more detail in the following section), the nominal stress-strain and strain rate responses are measured during testing, then fit to the JC framework to evaluate the parameters. Lesuer [25] conducted a series of SHB testing (both compressive and tensile) to evaluate the effectiveness of the JC formulation for use in simulating aircraft engine containment and impacts to aircraft structure from uncontained engine debris. He evaluated the response of Ti-6Al-4V specimens at strain rates of 4500 s^{-1} (compression) and 5200 s^{-1} (tension), and Al 2024-T3 specimens at 4000 (compression) s^{-1} and 8000 (tension) s^{-1}, with two repetitions per test case. New values for the parameters *A, B*, and n were calculated using the SHB data, while published data was used to calculate C. For the titanium alloy, the results indicate that the JC model with the new parameters was accurate to about 10^{3} s^{-1}. Above this strain rate, the flow stress was found to increase sharply with strain rate owing to a change in the deformation mechanics. For the aluminum alloy, on the other hand, good correlation between the predicted and measured flow stress was found

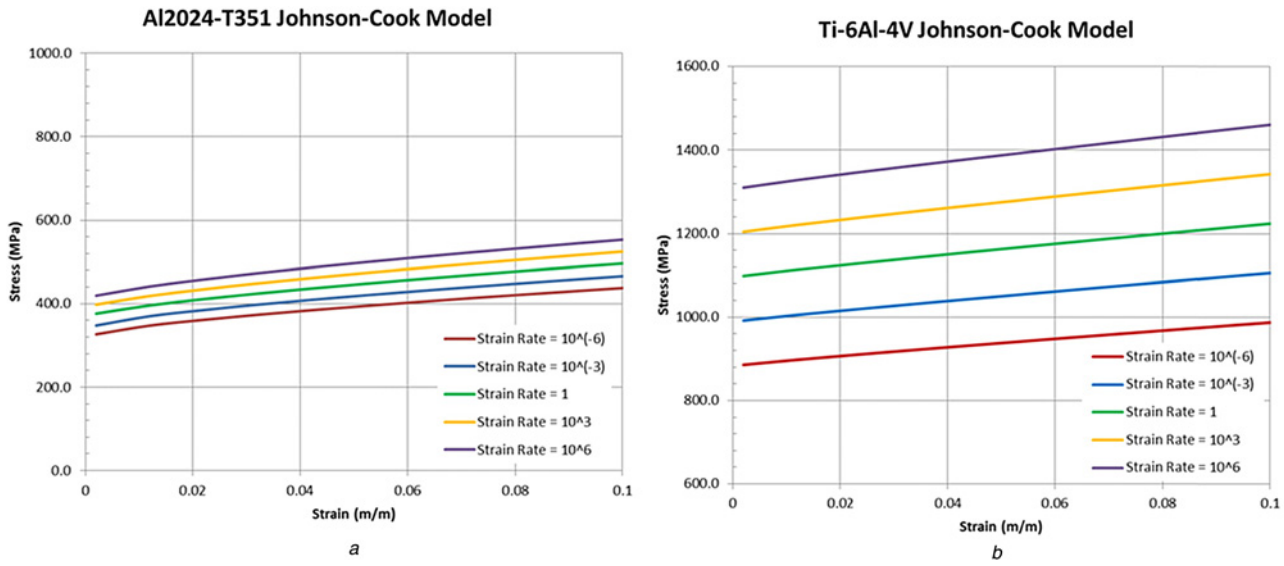

Fig. 2 *Johnson-Cook plots of yield stress as a function of strain rate for Al2024-T351 and Ti-6Al-4V*

J Eng 2015
doi: 10.1049/joe.2015.0118

Table 1 Johnson-Cook coefficients [25]

Material	*A*, MPa	*B*, MPa	*C*	*n*
Al2024-T351	369	684	0.014	0.93
Ti-6Al-4V	1098	1092	0.0083	0.73

throughout the entire range of measured strain rates ($\sim 10^4$ s^{-1}). The coefficients determined by Lesuer are shown in Table 1.

Although Lesuer's parameters show good correlation with test data at moderate strain rates, these rates are an order of magnitude lower than those experienced during an LP event. The parameters are also based on a limited data set, with only a single strain rate in tension and a single strain rate in compression. While previous research [10, 26] suggests that the JC model can be effective in simulating LP events, most studies have used comparisons with measured residual stresses from LP processing to establish validation. However, owing to uncertainties in stress measurements near the peened surface, it was desired to assess the JC model independent of LP. In the following sections we present the test results and associated modeling to evaluate the suitability of the JC model for predicting component response at extremely high strain rates.

3 Experimental approach

To assess the effectiveness of the JC model with Lesuer's coefficients, three series of tests were conducted for each of the alloys of interest, Al 2024-T351 and Ti-6Al-4V. The intent was to use multiple test techniques to capture a much broader range of strain rates than the capability of any particular test method alone: quasi-static compression tests to measure the stress-strain response at low strain rates (0.1–1 s^{-1}); SHB tests for the midrange strain rate response ($\sim 10^3$ s^{-1}); and flyer plate impact testing to assess the very high strain rate response ($\sim 10^5$ s^{-1}).

All materials were tested in the as-received condition. The Al 2024-T351 was purchased in two plate thicknesses, 6.35 mm (0.25 inch) and 12.7 mm (0.5 inch), and machined to size. The Ti-6Al-4V was received as a 22.35 mm (0.88 inch) thick plate. Physical properties assumed for the test materials are given in Table 2. All testing was conducted at the University of Dayton Research Institute in Dayton, OH.

3.1 *Quasi-static testing*

Quasi-static compression testing was performed for both alloys using a standard servo-hydraulic test frame. Button-shaped samples measuring 6.35 mm (0.25 inch) in diameter and 7.62 mm (0.30 inch) thick were fabricated in the through-thickness direction of the plates. Room temperature strain was measured using strain gages mounted 180° apart in the center of the gage section of the specimens and oriented in the thickness direction. The strain gages (Vishay Micro-Measurements EP-08-031-DE-120 bonded with M-Bond AE10 adhesive) were able to measure strains to about 8%. Compression tests at nominal strain rates of 0.01 s^{-1} and 1.0 s^{-1} with three replicates per strain rate were conducted for each alloy.

Table 2 Physical properties assumed for data reduction and analysis

Physical property	Ti-6Al-4V	Al 2024-T351
Density, kg m^{-3}	4424	2784
Bulk modulus, GPa	116	85.7
Shear modulus, GPa	41.9	20.2
Poisson's ratio	0.33	0.3
Longitudinal wave speed, m s^{-1}	6150	6360

Table 3 Summary of split Hopkinson bar testing

Material	Strain rate	Replicates
Al 2024-T351	700	3
	1050	3
	2100	4
Ti-6Al-4V	650	3
	1000	3
	2000	4

3.2 *Split Hopkinson bar testing*

High strain rate compression tests were conducted on both alloys using SHB testing with nominal strain rates of 500 s^{-1}, 1000 s^{-1}, and 2000 s^{-1}. All SHB specimens were 3.18 mm (0.125 inch) thick button shapes, fabricated in the through-thickness direction of the plates. The titanium specimens measured 3.18 mm (0.125 inch) in diameter, while the aluminum specimens were 6.25 mm (0.25 inch) in diameter.

A schematic of the SHB test setup is shown in Figure 3. The apparatus consists of a striker bar and two pressure bars – an incident bar a transmitter bar – mounted and aligned longitudinally in bearings for rigid support. The bars were fabricated from 12.7 mm (0.5 inch) diameter Inconel 718. The 0.76 m (2.5 ft) striker bar was launched from a gun barrel using compressed air. It strikes the 3.65 m (12 ft) incident bar, which initiates a stress pulse with a magnitude proportional to the striker bar velocity. The duration of the pulse, t_p, is equal to twice the acoustic transit time of the striker

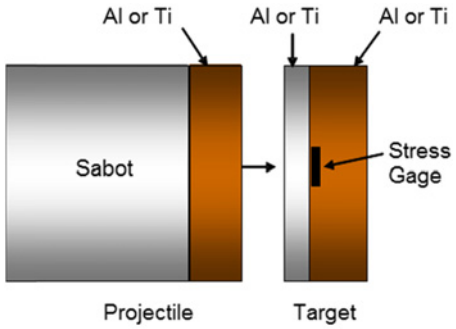

Fig. 4 *Schematic of flyer plate test setup*

Fig. 3 *Schematic of split Hopkinson bar test setup*

bar. For a striker bar of length l_s, the pulse duration is given by

$$t_p = \frac{2l_s}{C_o} \tag{2}$$

where C_o is the elastic wave velocity in the striker bar:

$$C_o = \sqrt{\frac{E}{\rho}} \tag{3}$$

with E and ρ the elastic modulus and density of the bar material, respectively. For the UDRI setup, t_p was about 306 μs using a value of 4968 m/s for the C_o of Inconel 718.

The test specimens were placed between the incident and transmitter pressure bars with a thin layer of Moly-disulphide lubricant on each side to eliminate friction between specimen/anvil interfaces. When the striker bar impacts the incident bar, a portion of the incident tensile pulse, ε_i, is transmitted through the specimen, ε_t, and the remainder is reflected back into the transmitter bar, ε_r. The amplitudes of the incident, reflected, and transmitted pulses were recorded by two Vishay Micro-Measurements CEA-06-250UW-10C 1000-Ohm strain gages bonded 180° apart on the pressure bars and 0.91 m (36 inch) away from the bar/specimen interface.

The average stress, strain, and strain rate responses of the specimen ($\sigma_s(t)$, $\varepsilon_s(t)$, and $\dot{\varepsilon}_s(t)$, respectively) were computed from the recorded strains in the pressure bars, assuming a uniform uniaxial stress state [27, 28]:

$$\begin{aligned} \sigma_s(t) &= E\frac{A_b}{A_s}\varepsilon_t(t) \\ \varepsilon_s(t) &= \frac{2C_o}{L}\int_0^t \varepsilon_r(t)dt \\ \dot{\varepsilon}_s(t) &= \frac{2C_o}{L}\varepsilon_r(t) \end{aligned} \tag{4}$$

Here, A_b and A_s are the cross-section areas of the pressure bar and the specimen in the gage section, respectively and L is the gage length of the specimen.

As shown in Equation (4), the computed average strain rate in the SHB tests depends on the magnitude of the reflected pulse. Assuming that the compressive strength of the material is constant, the magnitude of the reflected pulse will only depend upon the magnitude of the incident pulse. Thus, the specimen strain rate can be written as a function of the incident pulse only:

$$\varepsilon_i = \frac{1}{2E}C_o\rho V_s \tag{5}$$

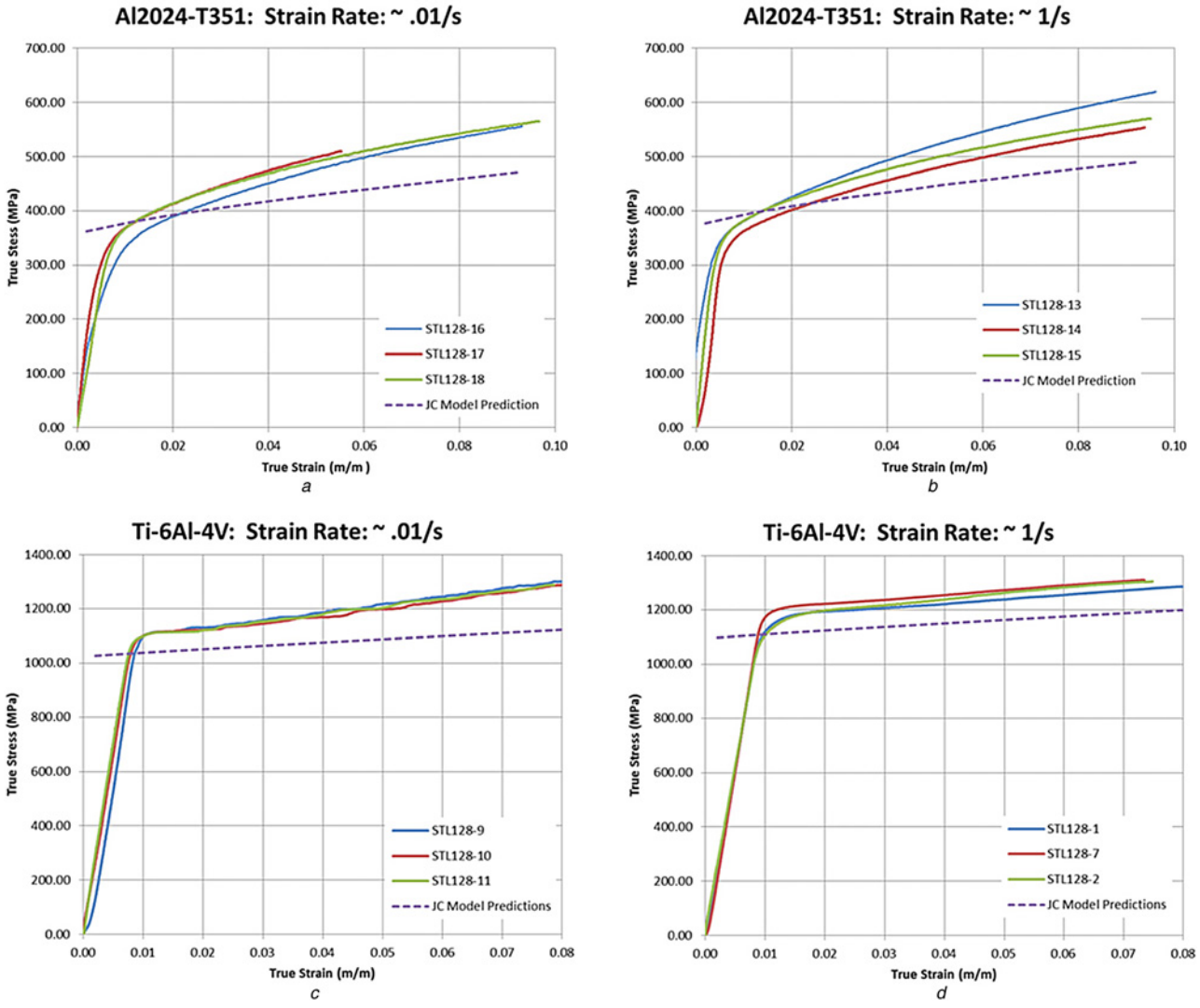

Fig. 5 *Comparison of JC model predictions and experimental results at low strain rates*

J Eng 2015
doi: 10.1049/joe.2015.0118

where V_s is the striker bar velocity. Consequently, the specimen response at different strain rates can be captured by using different striker bar velocities.

Using the SHB method as outlined above, compression tests on the two alloys were conducted at various strain rates under ambient conditions. A total of 20 SHB tests were performed as summarized in Table 3, with strain rates in the 700–2100 s^{-1} range for the aluminum and 650–2000 s^{-1} for the titanium.

3.3 *Flyer plate impact testing*

A series of flyer plate impact tests were designed to capture the strain rate response at rates higher than achievable with the SHB tests. A schematic of the flyer plate test setup used is shown in Figure 4. Target plates were fabricated from the specimen material using a thin cover plate (2–4 mm) and a thicker backing plate (4–8 mm) between which was embedded a manganin stress gage. The gage was sandwiched between two 25 μm mylar sheets to electrically insulate it from the cover and backing plates. The flyer (striker) plate was also fabricated from the specimen material and then attached to a plastic sabot prior to launch. Because of the relatively thick gage package in this configuration, rise times of the stress profile were relatively large. Nevertheless, peak shock stresses were measured with an estimated accuracy of ±3%.

The target assembly was securely fixed in a target tank with the impact surface situated perpendicular to the barrel of a 50 mm compressed gas/propellant gun, with launch velocities of 300–900 m/s. Details of the experimental technique are given in [29]. By varying the flyer plate impact velocity and the thicknesses of the flyer plate and target cover plate, strain rates in the range of 1–5 × 10^5 s^{-1} were achieved. The strain rate and shock stress in the target both decrease as the shock propagates deeper into the target until steady-state is reached. The method used to determine the shock stress from the measured manganin gage profile is given in [30].

As with the quasi-static and SHB testing, flyer plate impact tests were conducted with both Al 2024-T351 and Ti-6Al-4V, with the flyer and target plates fabricated in the thickness direction of the base material. Twenty tests were conducted, with 11 yielding successful results (Table 3). However, in four of these cases, indicated with an asterisk in the final column, the peak shock stresses are significantly above what would be reasonably expected during LP processing (2–3 times the HEL); hence, these data are not included in subsequent analyses.

4. Results and discussion

4.1 *Low strain rate response*

Figure 5 compares the JC model predictions with the stress-strain data from the quasi-static testing. The solid lines show the measured response

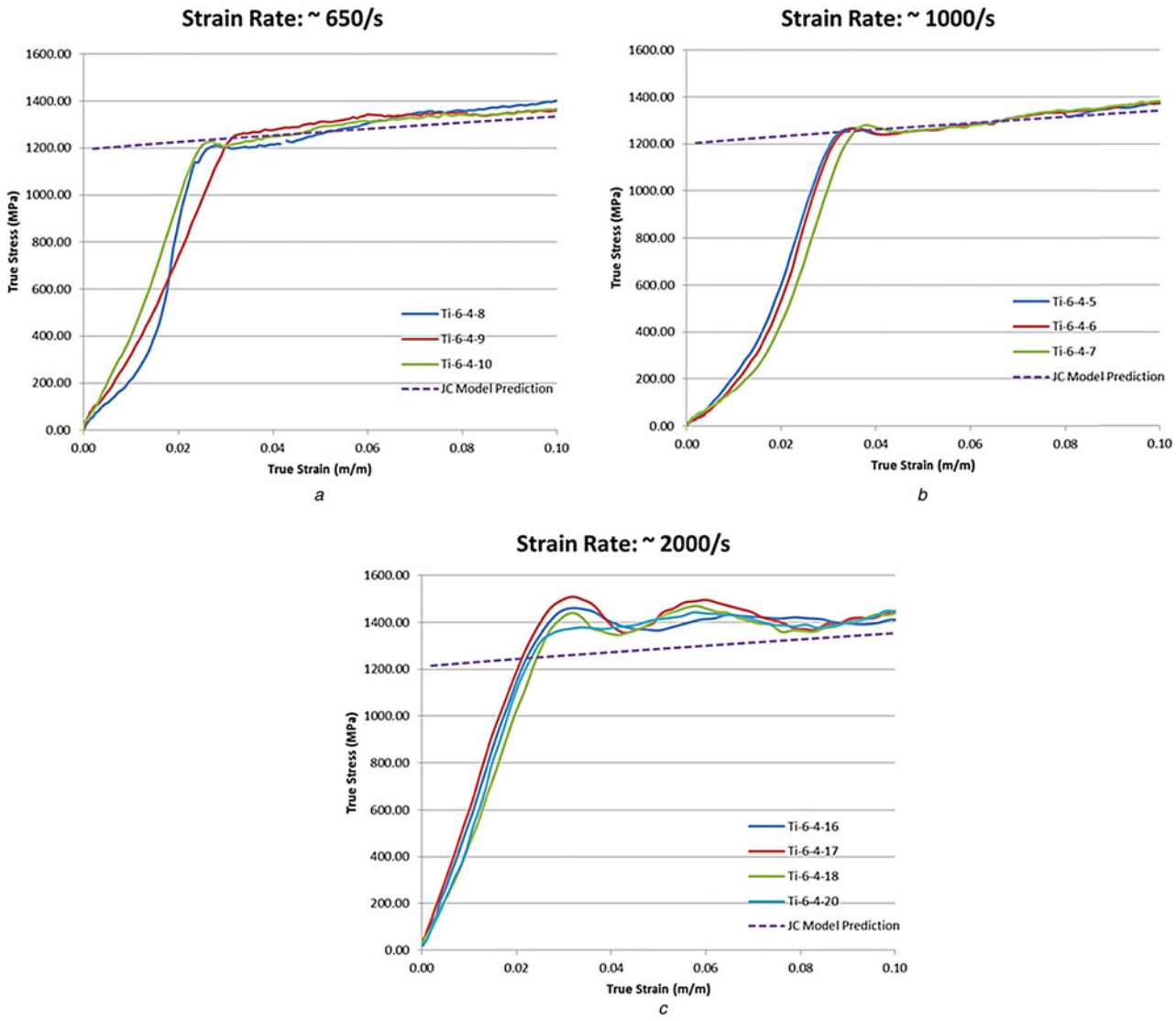

Fig. 6 *Comparison of JC model predictions with measured stress-strain response for Al 2024-T351*

doi: 10.1049/joe.2015.0118

for each test replicate while the dashed lines are the predicted stresses. As is seen, in all cases the model predictions are reasonable representations of the measured responses, although this can be largely attributed to the minimal strain rate dependence of these alloys at very low strain rates. At large plastic strains, on the order of 8% or more, the JC the model underpredicts the stresses by about 10–15%.

4.2 *Midrange strain rate response*

Comparisons with the JC model predictions for the midrange strain rate response, as measured using SHB testing, are shown in Figures 6 and 7 for the aluminum and titanium alloys, respectively. As in the previous section, the solid lines are the measured data and the dashed lines are the model predictions. Similar to the results at low strain rates, the JC model is a reasonable representation of the SHB results at moderately high strain rates. Because the JC coefficients were developed using strain rates in this range, these results provide a good verification of the basic model.

4.3 *High strain rate response*

To evaluate the effectiveness of the JC model [Equation (1)] at very high strain rates, FE simulations of the seven selected flyer plate tests (Table 3) were run using the commercial FE package Abaqus/Explicit and assuming the JC parameters determined by Lesuer [25]. All models were axisymmetric, with the projectile impacting the target at the recorded test velocity. In these simulations, only the flyer plate, the target, and the backing plate were modeled; the mylar sheets and the manganin gages were not included. Contact between the flyer plate and the target was included. The simulated shock stress at the model location corresponding to the manganin gage was evaluated and compared to the actual gage response.

A comparison of the simulated and measured responses for the aluminum specimens is shown in Figure 8 for three impact

Table 4 Summary of flyer plate testing

Material	Flyer plate thickness, mm	Target plate thickness, mm	Velocity, m s^{-1}	Peak shock stress, GPa
Al	2	2+gage+4	428	2.9
2024-T351	3	3+gage+6	335	2.3
	3	3+gage+6	589	5.3*
	3	3+gage+6	813	7.3*
	4	4+gage+8	326	2.3
	4	4+gage+8	972	9.3*
Ti-6Al-4V	2	2+gage+4	639	7.2
	3	3+gage+6	317	3.6
	3	3+gage+6	662	7.6
	3	3+gage+6	860	9.9*
	4	4+gage+8	421	4.8

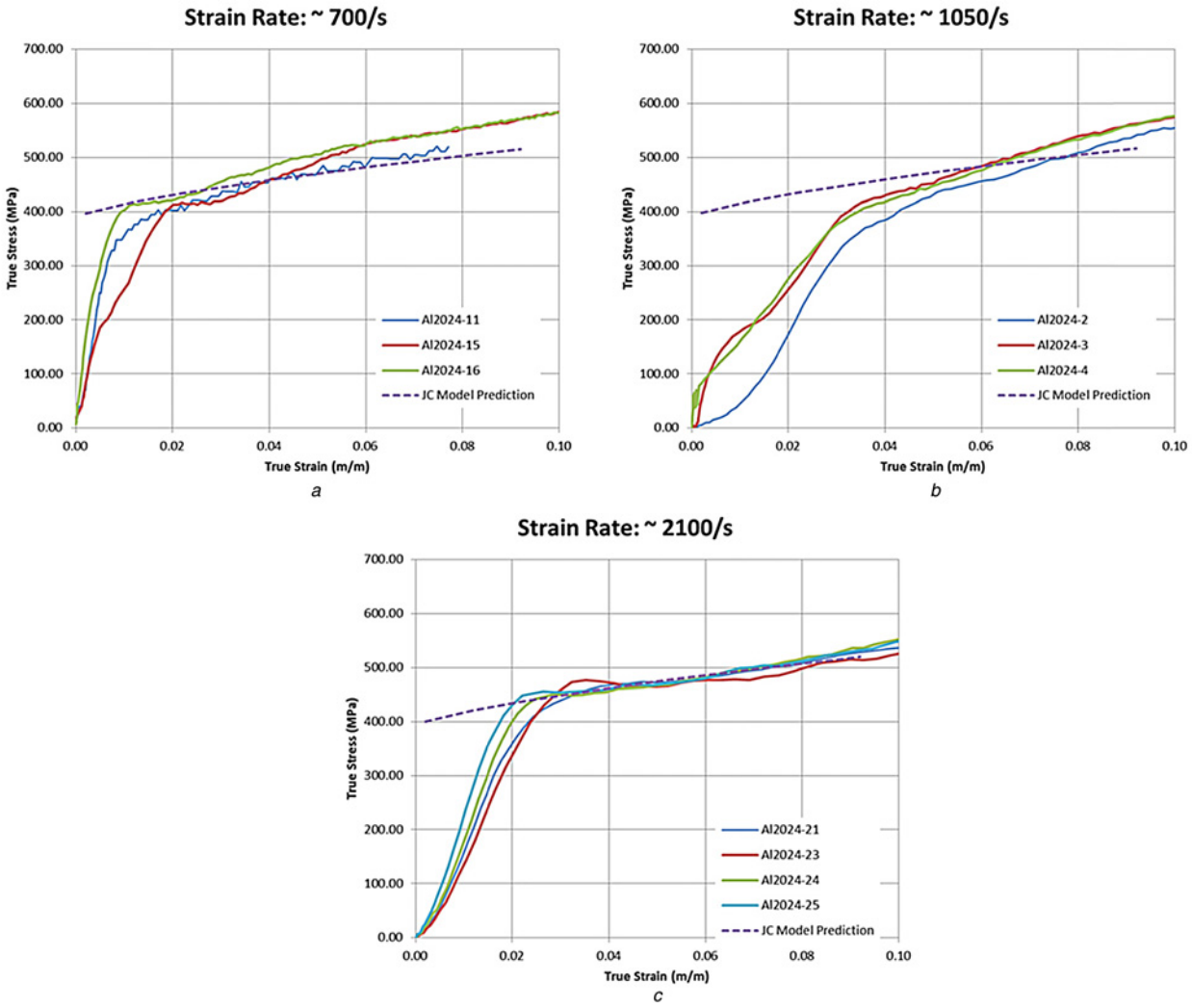

Fig. 7 *Comparison of JC model predictions with measured stress-strain response for Ti-6Al-4V*

J Eng 2015
doi: 10.1049/joe.2015.0118

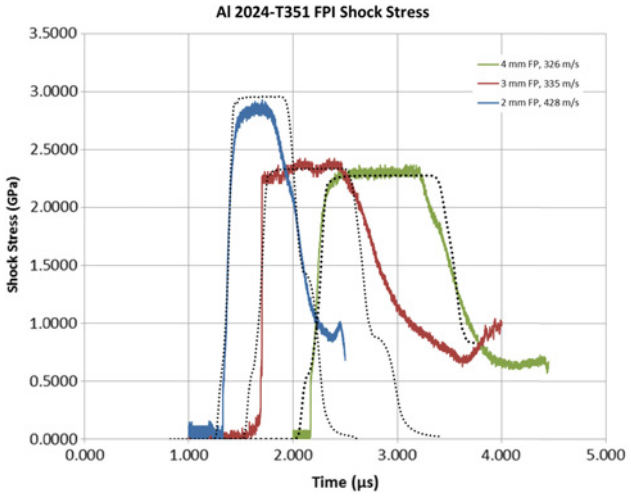

Fig. 8 *Comparison of the predicted and measured flyer plate impact shock response (Al 2024-T351)*

velocities. At these velocities, corresponding to peak shock stresses in the 2-3 GPa range, the correlation is very good. The model slightly over-predicts the measured peak stress at the higher shock stress, but only by about 5%.

Similar FE simulations were conducted for the titanium samples, again using the published Lesuer coefficients with a standard JC formulation. A comparison of the shock stresses as predicted by the model with the measured shock stresses is given in Figure 9. As can be seen, for this alloy the material model results in a small over-prediction of the shock response, on the order of about 10%.

To improve the correlation, the original JC material model was augmented to include a Mie-Grüneisen equation of state (EOS). In this adjusted model, the Hugoniot pressure and specific internal energy are assumed to be functions of density only. The implemented equation of state is linear in energy and assumes a linear relationship between the shock velocity U_s and the particle velocity U_p given by:

$$U_s = c_o + sU_p \tag{6}$$

where $s = 1.338$ for Al 2024-T351 and $s = 0.978$ for Ti-6Al-4V, and

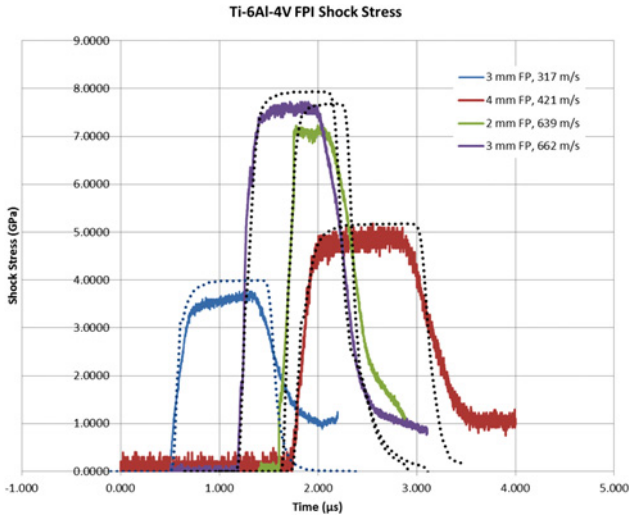

Fig. 9 *Comparison of the predicted and measured flyer plate impact shock response (Ti-6Al-4V)*

c_o is the bulk speed of sound:

$$c_o = \sqrt{\frac{K}{\rho}} \tag{7}$$

with K the elastic bulk modulus.

For the aluminum specimens, inclusion of the EOS had negligible effect on the predicted shock response for the range of shock stresses considered. For the titanium specimens, however, adding a Mie-Gruneisen EOS to the material model increased the over-prediction of the peak shock stresses, thereby worsening the correlation with the measured response. Although improvements might be possible with a nonlinear EOS, the basic JC model with Lesuer's parameters and without EOS augmentation are within 10% of the experimental values, which is sufficiently accurate for LP simulation.

5 Conclusions

1. The suitability of a Johnson-Cook material model developed using lower strain rate data was assessed for use in capturing the high strain rate response encountered during laser peen processing. Three series of tests for two material systems were conducted at low, mid, and high strain rates, and the experimental results compared to the Johnson-Cook model predictions.
2. In all strain rate regimes for both alloys, the correlations between measured and predicted stresses were assessed to be sufficiently accurate for simulation of the laser peen process.
3. An augmentation of the basic Johnson-Cook model with a linear equation of state was studied in an attempt to improve the correlation at very high strain rates, but had little to no effect on the predicted response.

6 Acknowledgments

All testing for this work was performed under Task Order #31 of the Structural Technology Evaluation and Analysis Program (STEAP) contract, Contract Number FA8650-04-D-3446, from General Dynamics Information Technology (GDIT). MEF is grateful for funding from the Lloyd's Register Foundation, a charitable foundation helping to protect life and property by supporting engineering-related education, public engagement and the application of research. Effort sponsored by the Air Force Office of Scientific Research, Air Force Material Command, USAF, under grant number FA8655-12-1-2084. The U.S. Government is authorized to reproduce and distribute reprints for Government purpose notwithstanding any copyright notation thereon. The views and conclusions contained herein are those of the authors and should not be interpreted as necessarily representing the official policies or endorsements, either expressed or implied, of the Air Force Office of Scientific Research or the U.S. Government.

7 References

[1] Peyre P., Fabbro R.: 'Laser Shock Processing: A Review of the Physics and Applications'. *Optical and Quantum Electronics*, 1995, **27**, (12), p. 1213–1229.

[2] Dorman M., Toparli M.B., Smyth N., Cini A., Fitzpatrick M.E., Irving P.E.: 'Effect of laser shock peening on residual stress and fatigue life of clad 2024 aluminium sheet containing scribe defects". *Materials Science and Engineering: A*, 2012, **548**, p. 142–151.

[3] Hill M.R., DeWald A., VanDalen J., Bunch J.: 'Design and analysis of engineered residual stress surface treatments for enhancements of aircraft stucture'. in The 2012 Aircraft Structural Integrity Program Conference, San Antonio, TX, 2012.

[4] Cai H., Bunch J., Polin L., Walker M., Garcia W.: 'Verification of analytical methodology to minimize inspection burdens and to utilize full benefits of residual stress life enhancement technique'.

in The 2013 Aircraft Structural Integrity Program Conference, Bonita Springs, FL, 2013.
[5] Air Force Research Laboratory Success Stories – A Review of 2011, 2001: Wright-Patterson Air Force Base, OH. p. 10.
[6] Coratella S., Sticchi M., Toparli M.B., Fitzpatrick M.E., Kashaev N.: 'Application of the eigenstrain approach to predict the residual stress distribution in laser shock peened AA7050-T7451 samples'. *Surface & Coatings Technology*, 2015, **2073**, p. 39–49.
[7] Braisted W., Brockman R.: 'Finite element simulation of laser shock peening'. *International Journal of Fatigue*, 1999, **21**, (7), p. 719–724.
[8] Ding K., Ye L.: "Three-dimensional dynamic finite element analysis of multiple laser shock peening processes". *Surface Engineering*, 2003, **19**, (5), p. 351–358.
[9] Ocaña J.L., Morales M., Molpeceres C., Torres J.: 'Numerical simulation of surface deformation and residual stresses fields in laser shock processing experiments'. *Applied Surface Science*, 2004, **238**, (14), p. 242–248.
[10] Singh G., Grandhi R.V., Stargel D.S., Langer K.: 'Modeling and optimization of a laser shock peening process'. 12th AIAA/ISSMO multidisciplinary analysis and optimization conference, 2008, p. 5838–5850.
[11] Brockman R.A., Braisted W.R., Olson S.E, *ET AL.*: 'Prediction and characterization of residual stresses from laser shock peening'. *International Journal of Fatigue*, 2012, **36**, (1), p. 96–108.
[12] Hasser P.J., Malik A.S., Langer K., Spradlin T.J.: 'Simulation of Surface Roughness Effects on Residual Stress in Laser Shock Peening'. in ASME 2013 International Manufacturing Science and Engineering Conference collocated with the 41st North American Manufacturing Research Conference: American Society of Mechanical Engineers.
[13] Arif A.F.M.: 'Numerical prediction of plastic deformation and residual stresses induced by laser shock processing'. *Journal of Materials Processing Technology*, 2003, **136**, p. 120–138.
[14] Peyre P., Chaieb I., Braham C.: 'FEM Calculation of residual stresses induced by laser shock processing in stainless steels'. *Modeling and Simulation in Materials Science and Engineering*, 2007, **15**, pp. 205–221.
[15] Warren A.W., Guo Y.B., Chen S.C.: 'Massive parallel laser shock peening: Simulation, analysis, and validation'. *International Journal of Fatigue*, 2008, **30**, (1), pp. 188–197.
[16] Ding K., Ye L.: 'Laser Shock Processing, Process Performance and Simulation'. (Boca Raton, FL, CRC Press, 2006).
[17] Montross C.S., Wei T., Ye L., Clark G., Mai Y.-W.: 'Laser shock processing and its effects on microstructure and properties of metal alloys: a review'. *International Journal of Fatigue*, 2002, **24**, (10), p. 1021–1036.
[18] Meyers M.A.: 'Dynamic Behavior of Materials' (John Wiley & Sons, New York, 1994).
[19] Bodner S.R.: 'Unified plasticity for engineering applications' (Mathematical Concepts and Methods in Science and Engineering, Springer, 2002).
[20] Miller A.: 'An inelastic constitutive model for monotonic, cyclic, and creep deformation, Part 1'. *ASME Journal of Engineering Materials and Technology*, 1976. **98**: p. 97–105.
[21] Bammann D.J., Chiesa M.L., Johnson G.C.: 'Johnson. Modeling large deformation and failure in manufacturing processes'. in International Congress of Theoretical and Applied Mechanics, Kyoto, Japan, 1996.
[22] Zerilli F.J., Armstrong R.W.: 'Dislocation-mechanics-based constitutive relations for materials dynamic calculations'. *Journal of Applied Physics*, 1987, **61**, (5), p. 1816–1825.
[23] Johnson G.R., Cook W.H.: 'A constitutive model and data for metals subjected to large strains, high strain rate and high temperatures', in Proceedings of the 7th International Symposium on Ballistics, The Hague, Netherlands, 1983, p. 541–547.
[24] Bhamare S., Ramakrishnan R.G., Mannava S.R., Langer K., Vasuvedan V.K., Qian D.: 'Simulation-based optimization of laser shock peening process for improved bending fatigue life of Ti-6Al-2Sn-4Zr-2Mo alloy". *Surface & Coatings Technology*, 2013. **232**: p. 464–474.
[25] Lesuer D.R.: Experimental Investigations of Material Models for T-6Al-4V Titanium and 2024-T3 Aluminum. 2000, Lawrence Livermore National Laboratory, Report No. DOT/FAA/AR-00/25.
[26] Amarchinta H.K., Grandhi R.V., Langer K., Stargel D.S.: 'Material model validation for laser shock peening process simulation'. *Modelling and simulation in materials science and engineering*, 2009, **17**, (1), p. 015010.
[27] Follansbee P.S.: 'The Hopkinson Bar, in Metals Handbook - Mechanical Testings' (ASM, Metals Park, OH, 1985), p. 198–203.
[28] LeBlanc M.M., Lassila D.H.: 'Dynamic tensile testing of sheet material using the split Hopkinson bar technique'. *Experimental Techniques*, 1993, **17**, (1), p. 37–42.
[29] Hopkins A., Brar N.S.: 'Hugoniot and shear strength of titanium 6–4 under shock loading'. AIP Conference Proceedings, 2000, **505**, (1), p. 423–426.
[30] Rosenberg Z., Yaziv D., Partom Y.: 'Calibration of foil-like manganin gauges in planar shock wave experiments'. *Journal of Applied Physics*, 1980, **51**, (7), p. 3702–3705.

J Eng 2015
doi: 10.1049/joe.2015.0118